Excitation-dependent carrier lifetime and diffusion length in bulk CdTe determined by time-resolved optical pump-probe techniques

Patrik Ščajev,[1,a)] Saulius Miasojedovas,[1] Algirdas Mekys,[1] Darius Kuciauskas,[2] Kelvin G. Lynn,[3] Santosh K. Swain,[3] and Kęstutis Jarašiūnas[4]
[1]*Institute of Photonics and Nanotechnology, Faculty of Physics, Vilnius University, Saulėtekio al. 3, LT 10257 Vilnius, Lithuania*
[2]*National Renewable Energy Laboratory, 15013 Denver West Parkway, Golden, Colorado 80401, USA*
[3]*Center for Materials Research, Washington State University, Pullman, Washington 99164, USA*
[4]*Faculty of Physics, Vilnius University, Saulėtekio al. 3, LT 10257 Vilnius, Lithuania*

(Received 26 October 2017; accepted 22 December 2017; published online 11 January 2018)

We applied time-resolved pump-probe spectroscopy based on free carrier absorption and light diffraction on a transient grating for direct measurements of the carrier lifetime and diffusion coefficient D in high-resistivity single crystal CdTe (codoped with In and Er). The bulk carrier lifetime τ decreased from 670 ± 50 ns to 60 ± 10 ns with increase of excess carrier density N from 10^{16} to 5×10^{18} cm^{-3} due to the excitation-dependent radiative recombination rate. In this N range, the carrier diffusion length dropped from 14 μm to 6 μm due to lifetime decrease. Modeling of in-depth (axial) and in-plane (lateral) carrier diffusion provided the value of surface recombination velocity $S = 6 \times 10^5$ cm/s for the untreated surface. At even higher excitations, in the 10^{19}–3×10^{20} cm^{-3} density range, D increase from 5 to 20 cm^2/s due to carrier degeneracy was observed. *Published by AIP Publishing.* https://doi.org/10.1063/1.5010780

I. INTRODUCTION

Owing to its optoelectronic and chemical properties, CdTe is an ideal material for thin film polycrystalline solar cells. The current power conversion efficiency record is 22.1%, and simulations indicate pathways to 25% efficient CdTe solar cells.[1] To achieve such efficiencies, modeling suggests that doping needs to reach 10^{16} cm^{-3}, carrier lifetime exceed 100 ns, and interface recombination velocity be reduced below 1000 cm/s.[1] Doping with Cu is limited by compensation,[2] but recent progress with P[3] and As[4] dopants suggests that $\geq 10^{16}$ cm^{-3} doping could be achieved. In this paper, we analyze other CdTe material properties required for high efficiency solar cells: carrier lifetimes, surface and bulk recombination, and carrier diffusion length.

In earlier studies of carrier lifetimes in CdTe,[5–7] it was generally assumed that the recombination process is determined only by the minority-carrier capture rates. However, when the electrons and holes are photoexcited in similar carrier densities by interband transitions, both the electron and hole capture processes should be considered, and the recombination rate is determined by the slower process.[8,9] Intrinsic defect governed recombination was analyzed using first-principles methods[10] and this analysis suggested the two-level recombination process in p-type CdTe, being mediated by the Te antisite defect, Te_{Cd}^{2+}, in different charge states. However, the previous experimental study[11] on semi-insulating CdTe revealed the very efficient electron capture due to Cd vacancy V_{Cd}^{2-} [which is a deep double acceptor at E_C – (0.6–0.7) eV with density of few times 10^{15} cm^{-3} (Ref. 12)]. The electrical activity of V_{Cd}^{2-} saturated with the photogenerated carrier concentration of $(3–5) \times 10^{15}$ cm^{-3} or after co-doping by shallow donors (such as Cl).[11] Recent observation of enhanced carrier lifetimes in CdTe layers after annealing in a Cd-rich atmosphere[13] indirectly supported the impact of Cd vacancies,[14] Te antisites[10] or their complexes.

Several groups have analyzed recombination in heteroepitaxial CdTe and bulk crystals using time-resolved photoluminescence (TRPL) with two-photon (2P) carrier generation.[5,15] In spite of the photoluminescence (PL) experiment being relatively simple and the radiative processes in CdTe strongly suppressed by fast nonradiative recombination, interpretation of TRPL data encounters some methodological problems. Determination of the carrier lifetime from TRPL decay kinetics requires validation of the radiative recombination mechanism at experimental conditions (monopolar or bipolar recombination), as well as analysis of the dependence of the radiative recombination coefficient on excitation.[16,17] Moreover, the photons generated by radiative recombination could be reabsorbed before escaping the CdTe layer and thus the photoluminescence (PL) emission spectrum is dependent on the sample thickness.[18] Consequently, the TRPL kinetics will be also changed due to reabsorption and exhibit a fast decay component because of carrier in-depth redistribution during the measurement.[15] As an example, the reabsorption of PL emission in GaN layers at 1P excitation resulted in two-times faster initial TRPL decay due to carrier in-depth diffusion.[19] Finally, in TRPL kinetics, the impact of reabsorption may interplay with fast surface recombination, which is rather strong in CdTe[20] and requires technological solutions for surface passivation.[18]

The optical pump-probe techniques directly measure the carrier lifetime and diffusivity D at various carrier densities, thus providing the carrier diffusion length—the key parameter for charge collection in solar cell materials. The

a)Electronic mail: patrik.scajev@ff.vu.lt

pump-probe techniques, similar to TRPL, also explore interband carrier generation using a 1P or 2P excitation, but enable optical monitoring of the total carrier density, as an infrared probe integrates the instantaneous density of nonequilibrium carriers over the sample depth. Namely, light induced free carrier absorption (FCA) and light diffraction on transient gratings (LITGs) enable monitoring of light-induced probe-beam absorption or its refraction by the excess carriers. These techniques have been applied to determine the carrier lifetimes, diffusion coefficients, and carrier diffusion lengths in GaN bulk crystals and epitaxial layers,[21,22] SiC,[23] diamond,[24] InGaN or AlGaN quantum wells,[25] and enabled measurements of surface recombination velocities in III-V compounds.[21] For semiinsulating CdTe, LITG was applied to investigate carrier generation from the deep vanadium impurity,[11] allowed determining the type of photogenerated carriers from the deep impurities,[26] and enabled analysis of the deep-trap contribution to recombination in the presence of additional fast recombination centers.[27]

In this paper, we report carrier dynamics in the bulk of single crystal CdTe in a wide range of excess carrier density (from 10^{16} to 10^{21} cm^{-3}). Monitoring the fast and slow carrier dynamics from a few ns up to a few μs, we determined the carrier diffusion coefficient D, carrier lifetime, and diffusion length. Numerical solution of the continuity equation using the D and carrier lifetime determined from LITG provided a large value of surface recombination velocity ($S = 6 \times 10^5$ cm/s) of the untreated surface. Comparative study of PL emission spectra at 1P and 2P excitation allowed evaluation of the radiative lifetime, its saturation at high injection, and impact on the carrier diffusion length.

II. SAMPLES AND TECHNIQUES

Single crystal CdTe was grown at the Washington State University using the Vertical Bridgman Method.[3,4] Dislocation densities for similar samples were 2–5 $\times 10^4$ cm^{-2}. For optical measurements, we selected an In ($\approx 3 \times 10^{17}$ cm^{-3}) and Er (1.5×10^{17} cm^{-3}) co-doped high-resistivity 0.5 mm thick crystal. It is believed that the compensation arises due to simultaneous impact of the shallow indium donor at $E_C - 14$ meV (Ref. 28), as well as a 120–150 meV In-A acceptor[29] and two intrinsic deep defects (the Te antisite and the Cd vacancy in different charge states).[12,30] Co-doping with Er allows for a deep level at 0.8 eV that removes the V_{Cd}^{2-} type complexes with the Te antisite or their complexes. Er provides a shallow acceptor level at 72 meV.[31]

The preliminary PL measurements at 2P excitation (1120 nm, Ref. 32) revealed that the sample properties are uniform. Hall mobility measurements (with ohmic In contacts) provided $\mu_H = 500 \pm 50$ cm^2/V s, Hall factor $r_H = 1.18$, $\mu_e = 420 \pm 40$ cm^2/V s, and $n_0 = (1.2 \pm 0.1) \times 10^9$ cm^{-3} at 300 K. Temperature change of the electron concentration provided 0.76 ± 0.05 eV activation energy (in 300–400 K interval n_0 increased up to 10^{11} cm^{-3}) which should correspond to the midgap deep acceptor (tentatively we attribute it to the Te antisite and the Cd vacancy complex at 0.79 ± 0.06 eV,[30] with 1.58×10^{-12} cm^2 capture cross section).

Two optical pump-probe techniques (LITG and FCA) were used with 1P ($\lambda_{2h} = 527$ nm, 2nd harmonic of the Nd:YLF laser) and 2P (1053 nm, 1st harmonic of the Nd:YLF laser) excitation. For LITG, the excitation beam was split by a diffractive optical element (a permanent diffraction grating with a fixed spatial period), and two diffracted beams, intersecting at an angle Θ, created an interference pattern with a period $\Lambda \approx \lambda_{2h}/\sin(\Theta)$ in the sample.[33] The light-induced spatial modulation of carrier density $\Delta N \propto (1 + \cos(2\pi x/\Lambda))$ was monitored by the diffraction of a probe beam at wavelength $\lambda_{probe} = 1053$ nm. The probe beam diffraction efficiency η and its decay are governed by the refractive index modulation Δn by ΔN, and $\Delta n\,(x,z,t) = n_{eh}\,\Delta N(x, z, t)$ integrated over the sample depth d gives the expressions for the diffraction efficiency η and the grating decay time τ_G

$$\eta(t) = \left(\frac{2\pi\Delta n d}{\lambda_{probe}}\right)^2 = \left(\frac{2\pi n_{eh}\int_0^d \Delta N dz}{\lambda_{probe}}\right)^2 \exp\left(-\frac{2t}{\tau_G}\right), \quad (1a)$$

$$\frac{1}{\tau_G} = \frac{1}{\tau_R} + \frac{1}{\tau_D}. \quad (1b)$$

Here, t is the probe beam delay time, n_{eh} is the refractive index change for one electron-hole pair, $\tau_D = \Lambda^2/4\pi^2 D$ is the grating diffusive time, τ_R is the recombination time, and $d = 0.5$ mm is the sample thickness. By measuring the grating decay rates $1/\tau_G$ at different Λ, we determined D and fast components of τ_R according to Eq. (1b).

The slow component of carrier lifetime was measured from differential transmissivity (DT) caused by the free carrier absorption. Carriers were generated by 2P excitation, and the DT for the probe beam (at 1053 nm) is described by[34]

$$\ln\left(T_0/T(t)\right) = \sigma_{eh} d \frac{N_{02P}\exp\left(-t/\tau_R\right)}{1 + bdI_0}. \quad (2)$$

Here, σ_{eh} is the free carrier absorption cross section at probe wavelength, ΔN_{02} is the carrier density under 2P excitation: $\Delta N_{02} = \int_{-\infty}^{+\infty} \beta P(t)^2 dt/2h\nu = bI_0^2/2h\nu$, where β (cm/GW) is the two-photon absorption coefficient and $P(t) = 2I_0\exp(-4t^2/\tau^2_{1h})\pi^{-1/2}\tau_{2h}^{-1}$ (GW/cm^2) is the excitation beam instantaneous power density.[34] The factor $b = \beta/\left(\tau_{1h}\sqrt{\pi/2}\right)$[34] describes a decrease of the pump beam intensity $I(z)$ during its propagation in the crystal (here, τ_{1h} is the excitation pulse full width at 1/e intensity)

$$I(z) = \frac{I_0}{1 + bzI_0}. \quad (3)$$

Similarly, the depth profile of carrier density $\Delta N(z)$ is given by

$$\Delta N(z) = \frac{\Delta N_{02}}{(1 + bzI_0)^2}. \quad (4)$$

These models allowed us to calculate an average carrier density at 2P generation. For lifetime measurements (single

2P beam excitation), it was equal to $\Delta N_{av,FCA} = \Delta N_{02}(1 + bdI_0/2)/(1 + bdI_0)$. For diffusion measurements (two 2P beam excitation), the ΔN_{av} value was larger by a factor 1.5 because of the nonsinusoidal profile of light-induced grating at two photon absorption (TPA) excitation conditions.[34] The excitation spot diameter in LITG and FCA measurements was 620 μm (at 1/e width). A smaller probe with a diameter of 140 μm was used for both LITG and DT to monitor the homogeneous central part of the excitation spot.

The pump beam penetration depth δ under 1P excitation $\delta = \alpha^{-1}{}_{1P}$ is determined by the absorption coefficient at 527 nm, where $\alpha_{1P} = 9.3 \times 10^4\,cm^{-1}$.[35] The carrier density near the surface was calculated as $\Delta N_{01P} = \alpha_{1P} I_0/h\nu$,[36] where $I_0 = (1–R)I_{inc}$ is the excitation energy density in the sample (in mJ/cm^2), R is the reflection coefficient, I_{inc} is the incident excitation density, and $h\nu$ is the photon energy. The average over-depth carrier density is $\Delta N = \Delta N_{01P}/2$.[36]

PL measurements were performed in a standard backscattering geometry using a Hamamatsu streak camera and an Acton monochromator.

III. RESULTS AND DISCUSSION

A. Carrier dynamics with 2P generation: Carrier diffusion and scattering mechanisms

Using 2P generation, we analyzed carrier diffusivity and lifetime in the semiconductor bulk. We first describe the determination of the carrier density with 2P excitation.

Figure 1(a) shows the probe beam transmission (DT) and its diffraction efficiency (DE) from the transient grating. The superlinear DT and DE dependence on the excitation fluence I_0 confirmed the carrier generation by 2P absorption, as the carrier density ΔN (DT $\propto \Delta N$) increases quadratically with I_0. The slope for DE(I_0) is nearly two times larger because of the quadratic dependence of DE vs. carrier density [DE $\propto \Delta N^2$, see Eq. (1)]. The decrease of DT slope at $I_0 > 20$ mJ/cm^2 is due to absorption saturation [described by Eq. (4)] and due to absorption of pump by free carriers. Much stronger DE drop at $I_0 > 10$ mJ/cm^2 is mainly due to the strongly nonsinusoidal grating profile thus reducing the modulation depth and LITG efficiency. Fitting of the DT (I_0) data provided the cross section of free carrier absorption, $\sigma_{eh} = 2.1 \times 10^{-17}$ cm^2. The value of σ_{eh} is mostly determined by the hole absorption, as the reported value of free electron absorption in CdTe is much smaller [$\sigma_e = 1.4 \times 10^{-19}$ cm^2 (Ref. 37)]. On the other hand, the diffraction efficiency η is governed by the refractive index change Δn [see Eq. (1)], which mainly depends on the electron density: $\eta \propto \Delta n^2 \propto (N_e/m_e + N_h/m_h)^2$, as $m_e < m_h$.

In order to determine the carrier density ΔN_{02}, the laser pulse duration and two-photon absorption coefficient must be determined. The laser pulse duration was measured by autocorrelation of laser pulses [i.e., by the second harmonic generation in the potassium dihydrogen phosphate (KDP) crystal]. The fit with the Gaussian function provided the laser pulse duration of 13.4 ps at 1/e intensity [see Fig. 1(c)]. In turn, the measurements of pump beam transmission [Fig. 1(b)] and fitting of this data to $I_T(I_0)/I_T(0) = \ln(1 + bdI_0)/(bdI_0)$ provided the values b = 1.5 cm/mJ and $\beta = 25.5$ cm/GW at 1053 nm. The β value is very close to previously reported $\beta = 26$ cm/GW at 1064 nm.[38] This data allowed us to estimate that with 2P excitation, the carrier densities varied from 10^{16} to 5×10^{18} cm^{-3}.

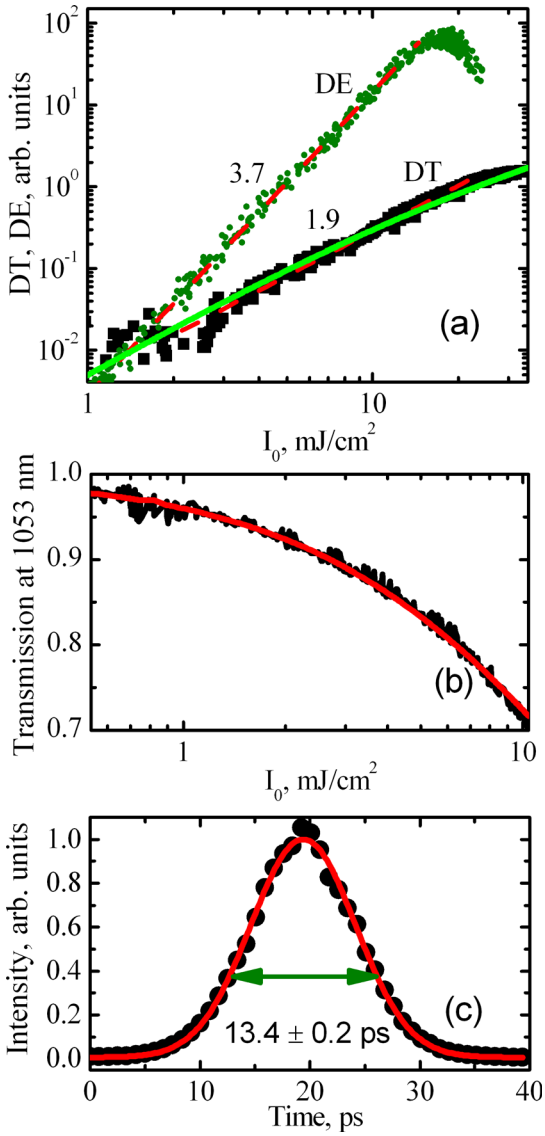

FIG. 1. (a) Probe beam differential transmission (DT) and diffraction efficiency (DE) dependence on the excitation fluence I_0; (b) pump beam transmission dependence on the excitation fluence. The solid lines in (a) and (b) are the analytic fits and the dashed lines are the linear fits with slope values indicated. 2P excitation was at 1053 nm; (c) excitation pulse and its fit with the Gaussian function (13.4 ps width at 1/e intensity).

Next, we consider carrier diffusion. Figure 2(a) shows the LITG decays for the grating period of 3.9 μm. The grating decay is single exponential and becomes faster with excitation increase. Assuming that the grating decay is governed by lateral diffusion [$\tau_G = \tau_D \ll \tau_R$, see Eq. (1b)] and that recombination time is much longer, the values of the diffusion coefficient $D = \Lambda^2/4\pi^2\tau_D$ were determined [circles in Fig. 2(b)]. The measurements of LITG decays for the grating period of 2.3 μm provided nearly the same values of D [squares in Fig. 2(b)] confirming the diffusive grating decay.

In the general case, the value of D in bipolar-like plasma is determined by a ratio of electrons and holes, according to (D_e and D_h are diffusivities for electrons and holes)

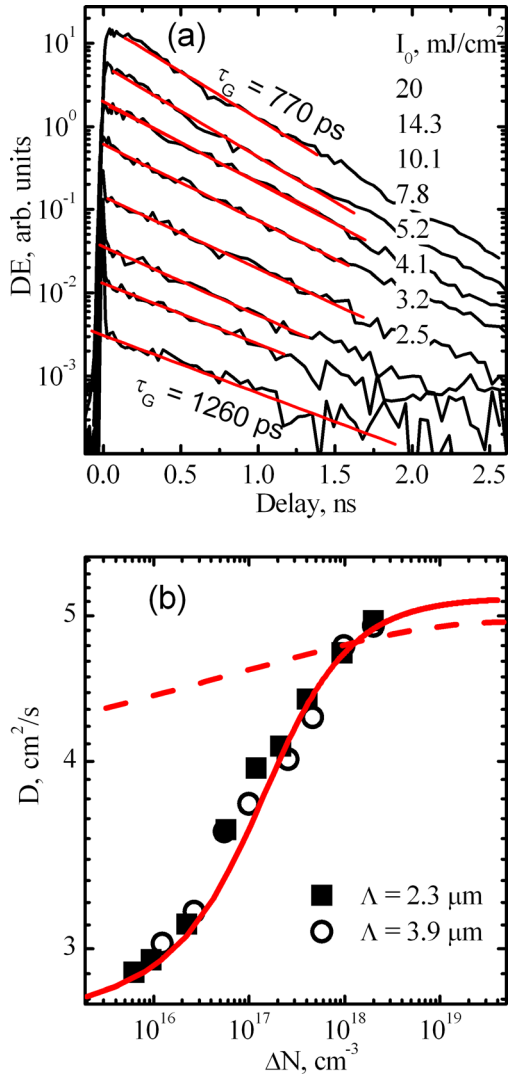

FIG. 2. (a) 2P excitation LITG kinetics measured with a grating period of 3.9 μm for excitation fluences I_0 shown in the legend. (b) Values of the bipolar diffusion coefficient D at various excess carrier densities ΔN. In (b), the dashed line shows a fit using a model based on ionised impurity scattering. A solid line shows a fit based on ionised impurity scattering and neutralization of shallow acceptors.

$$D = \frac{(n+p)}{p/D_e + n/D_h}. \tag{5}$$

Assuming that during LITG measurements electrons remain free, but holes are partially captured by acceptors, we estimated the ionized acceptor concentration according to Ref. 39

$$N_A{}^- = \frac{N_A}{g\Delta N/N_{VT}+1}, \quad N_A = N_A{}^- + N_A{}^0, \quad N_{VT} = N_V e^{\frac{-E_A}{k_B T}}. \tag{6}$$

Here, g = 4 (Ref. 40) is the degeneracy factor for the acceptor level, E_A is the acceptor ionization energy, and $N_V = 2\times10^{19}\,\mathrm{cm}^{-3}$ is the density of states in the valence band. The concentration of free holes is expressed by $p = \Delta N - N_A + N_A{}^-$,[41] while the reduced diffusion coefficient D^R due to hole capture to acceptors (when all electrons remain free) is described as $D^R(\Delta N) = D(\Delta N)\times p/\Delta N$.[41] In the fit of $D^R(\Delta N)$ data in Fig. 2(b) by Eqs. (5) and (6), we assumed a shallow acceptor at $E_A = 62\pm5$ meV with density $N_A = 1.3\times10^{17}\,\mathrm{cm}^{-3}$ ($\mu_h = 110\,\mathrm{cm}^2/\mathrm{V\,s}$, and $\mu_e = 1045\,\mathrm{cm}^2/\mathrm{V\,s}$). The reduction of the scattering center concentration $N_A{}^+$ due to acceptor filling was also taken into account. Calculations provided n/p = 1.4 ratio at $10^{16}\,\mathrm{cm}^{-3}$ carrier density. Considering that Er creates a shallow acceptor level at $E_V + 71$ meV (Ref. 31) and the Er dopant density in our sample ($1.5\times10^{17}\,\mathrm{cm}^{-3}$) is very close to the estimated activation energy ($E_A = 62\pm5$ meV) and ionized acceptor density ($N_A = 1.3\times10^{17}\,\mathrm{cm}^{-3}$), we attributed their origin to Erbium. This result strongly supports the assumption that the shallow Er acceptor plays a significant role in diminishing mobility at low carrier densities [similarly as Al acceptors in compensated SiC (Ref. 41)] Nevertheless, an impact of deeper In-A center with 120–140 meV activation energy[29] cannot be excluded.

B. Carrier lifetimes and diffusion length

To determine the charge carrier lifetimes, we measured free carrier absorption (FCA) decays. In Fig. 3(a), we present

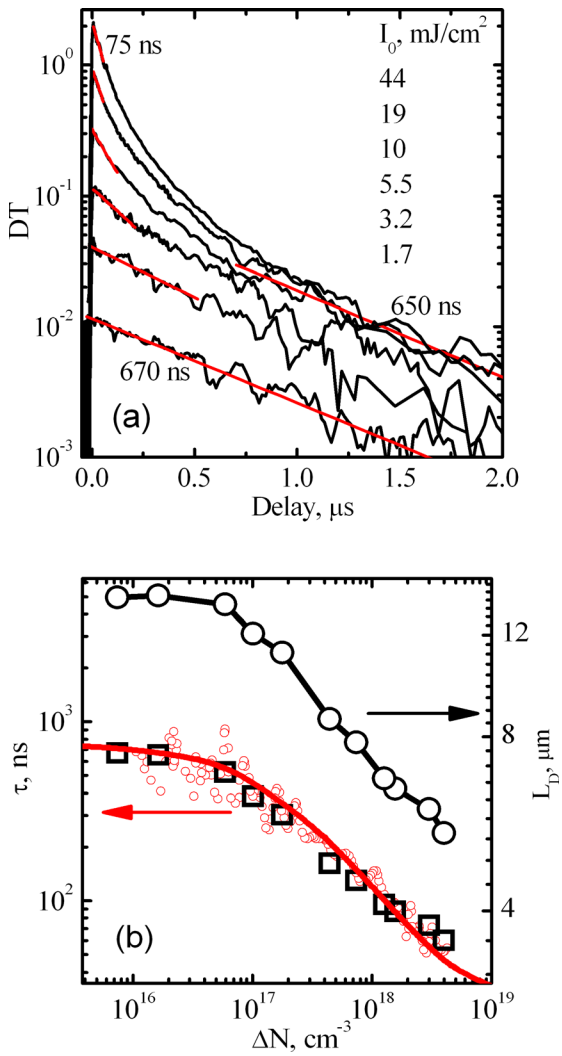

FIG. 3. Differential transmittance (DT) from the FCA decays (a), carrier lifetime τ, and diffusion length L_D (b). The solid lines are fits to the curves. The circles in (b) show the instantaneous carrier lifetime calculated as $\tau_{inst} = DT(t)/[dDT(t)/dt]$ using decay data at the highest excitations from (a).

DT kinetics, where the DT decay at low excitation conditions ($\Delta N = 1–3 \times 10^{16}\,cm^{-3}$) is single-exponential with 670 ns lifetime. The TRPL lifetime for the same sample is approximately two times shorter, 360 ns, because $PL \propto BN^2 \propto \exp(-2t/\tau)$. The carrier recombination time as measured by DT strongly decreased at $\Delta N > 10^{17}\,cm^{-3}$ and exhibited the fast decay component in the 1 μs time domain. We attribute the fast component to the radiative recombination,[42] which is analyzed below.

The lifetime excitation dependence $\tau(\Delta N)$ in Fig. 3(b) was analyzed using $1/\tau = 1/\tau_{NR} + B_{rad2P}(\Delta N)\Delta N$, where $\tau_{NR} = 700$ ns is the nonradiative lifetime. As described in Sec. III C, the radiative recombination coefficient B_{rad2P} is density-dependent.

Using the density-dependent τ [Fig. 3(b)] and D [Fig. 2(b)] values, we calculated the carrier diffusion length $L_D = (D(\Delta N)\tau(\Delta N))^{1/2}$ shown in Fig. 3(b). We found $L_D = 14\,\mu m$, when $\Delta N \le 3 \times 10^{17}\,cm^{-3}$. Materials with such diffusion length would be suitable for high efficiency thin film solar cells where carrier collection is by diffusion. L_D starts to decrease at $\Delta N > 10^{17}\,cm^{-3}$ and drops from 14 μm to 5.5 μm. In other studies, the minority hole and electron diffusion lengths were 1.75 μm,[43] 0.4–2 μm,[44] 1.8 μm,[45] 1.5–7.5 μm,[44] and 1.6 μm.[45] Diffusion length in the semi-insulating single crystal studied here is much higher due to the much longer carrier lifetime, presumably due to the low nonradiative defect density.

C. Analysis of radiative recombination

We now analyze radiative recombination, which impacts our results at high excitation densities. At high carrier densities, the radiative recombination coefficient B becomes density-dependent due to the state filling. This leads to reduced radiative recombination rate. The $B(\Delta N)$ dependence is described by[46]

$$B(\Delta N) = B_{rad}\frac{8\int_0^\infty \sqrt{x} f_e\left(m_{eh}/m_e x - x_{fe}\right) f_h\left(m_{eh}/m_h x - x_{fh}\right) dx}{9F_{1/2,e} \times F_{1/2,h}}. \quad (7)$$

Here, f_e and f_h are the electron and hole Fermi distribution functions, $x_f(\Delta N) = E_{Fe,h}/kT$ is the normalized Fermi energy level calculated using the Nilsson approximation, including the $\Delta N/N_{DOS}$ variable parameter.[47] The density of states N_{DOS} was calculated by $N_{DOS,\ e,h} = (m_{e,h}/m_0)^{3/2} \times 2.8 \times 10^{19}\,cm^{-3}$,[47] where m_{eh} is the reduced effective mass ($1/m_{eh} = 1/m_e + 1/m_h$). A simplified approximation to Eq. (7) can also be used[16]

$$B(\Delta N) = \frac{B_{rad}}{1 + \Delta N/N_b}, \quad (8)$$

where N_b represents the material-specific carrier density at which $B(\Delta N_b)$ becomes two times smaller than B_{rad}. Here, $B_{rad} = 3.8 \times 10^{-10}\,cm^3/s$ (Ref. 48) is numerically calculated by the Roosbroek and Shockley model[49] using the typical values of $m_e = 0.11$ and $m_h = 0.4$ for CdTe. In turn, the calculations by Eq. (7) provided $N_b = (7 \pm 0.4) \times 10^{18}\,cm^{-3}$ valid in the 10^{16}–$10^{20}\,cm^{-3}$ range.

Decrease of the radiative recombination rate at higher excitation leads to gradual saturation of the PL intensity, and this tendency was observed experimentally [Fig. 4(a)]. Fitting of the peak PL intensity in Fig. 4(a) with $PL \propto I_0^2/(1 + \Delta N_{avPL}/N_b)$ (taking into account that the PL carrier density is $\Delta N_{avPL} = \Delta N_{01P}/4$) due to the carrier degeneracy provided a similar value, $N_b = (6 \pm 2) \times 10^{18}\,cm^{-3}$.

Comparison of the PL emission spectra measured with 1P and 2P excitation [Fig. 4(b)] allowed us to analyze reabsorption and determine the effective radiative recombination coefficients for the bulk and near-surface excitation. Emission spectra were excitation-independent for both 1P and 2P with ΔN up to $10^{18}\,cm^{-3}$. This data can be used to provide $B_{rad2P}/B_{rad} = \text{Integral}(PL_{2P})/\text{Integral}(PL_{1P}) = 29$. Due to the fast surface recombination, the carriers at 1P excitation are confined near the surface and emitted photons are not reabsorbed, thus 1P excitation data reflects the real emission spectrum. (The

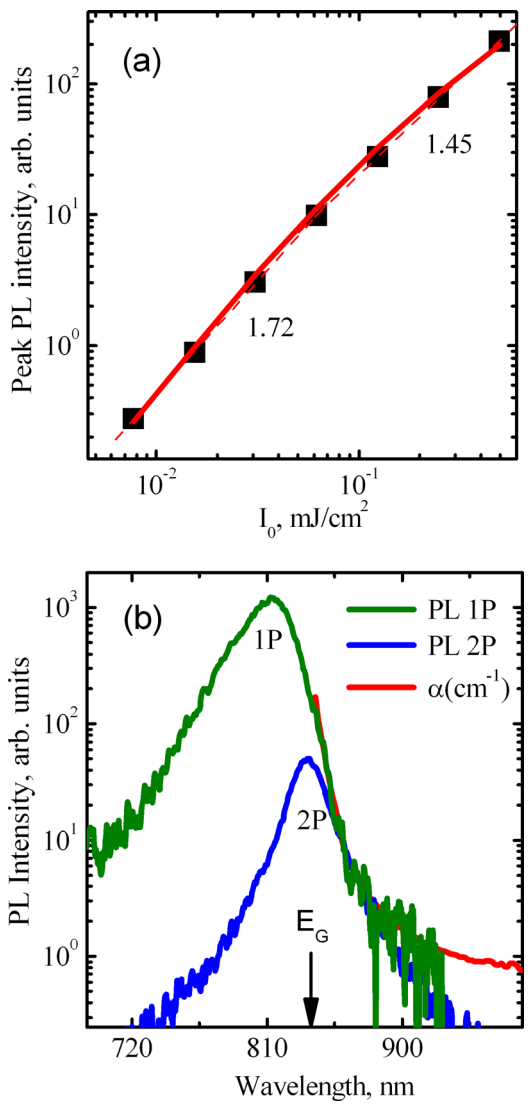

FIG. 4. (a) Peak PL intensity dependence on excitation fluence I_0 at 1P (527 nm) excitation. (b) PL emission spectra measured with 2P ($\Delta N = 10^{18}\,cm^{-3}$) and 1P ($\Delta N = 10^{18}\,cm^{-3}$) excitation and their relation to the measured absorption coefficient α. PL peak shifts from 813 nm (1P) to 836 nm (2P) due to reabsorption. An arrow indicates the CdTe bandgap at 1.48 eV.

reabsorption coefficient at the bandgap is $3 \times 10^4\,\mathrm{cm}^{-1}$, while for the 1P excitation at 527 nm $\alpha = 9.4 \times 10^4\,\mathrm{cm}^{-1}$,[35] i.e., the excitation depth is three times shorter than the reabsorption depth.) The fit to experimentally measured dependence $1/\tau(\Delta N) = 1/\tau_{NR} + B_{rad2P0}\Delta N/(1 + \Delta N/N_b)$ [Fig. 3(b)] provided $N_b = (7 \pm 1) \times 10^{18}\,\mathrm{cm}^{-3}$ and $B_{rad2P0} = (0.8 \pm 0.1) \times 10^{-11}\,\mathrm{cm}^3/\mathrm{s}$. Hence, from the data in Figs. 3(b) and 4(b), we find $B_{rad} = 2.4 \times 10^{-10}\,\mathrm{cm}^{-3}$, being close to the theoretical, $B_{rad} = 3.8 \times 10^{-10}\,\mathrm{cm}^3/\mathrm{s}$.[48] Nevertheless, at 1P excitations not all emission escapes the sample (limited by the escape cone and emission direction in the bulk), thus the B_{rad1P} value is lower. As an example, $B_{rad1P} = 10^{-10}\,\mathrm{cm}^{-3}$ value was obtained for surface PL excitation.[42]

According to Eq. (8), the radiative lifetime will saturate to $\tau = 1/B_{rad}N_b$. Therefore with 2P excitation, the radiative lifetime will saturate at 18 ns (using $B_{rad2P0} = (0.8 \pm 0.1) \times 10^{-11}\,\mathrm{cm}^3/\mathrm{s}$), and with 1P excitation, the radiative lifetime will saturate at 1.4 ns [using $B_{rad1P} = 10^{-10}\,\mathrm{cm}^{-3}$ (Ref. 42)]. Actually a similar 1P lifetime of $\tau_{PL} = 1.6$ ns was observed in samples with a low surface recombination velocity.[5]

D. Carrier dynamics with 1P excitation

We extended our analysis to even higher excess carrier densities from 10^{19} to $10^{21}\,\mathrm{cm}^{-3}$ with 527 nm (1P) excitation. Similar to 2P excitation measurements, we used the LITG technique to record the transient grating and monitor its decay. The measurements at some grating periods allowed direct determination of carrier diffusion coefficients and recombination rates. The initially excited near-surface layer of about 100 nm increased with time up to few micrometers, and the spatio-temporal carrier distribution was governed by diffusion and surface recombination.

In Fig. 5, we present the LITG decay kinetics for the grating periods $\Lambda = 1.25$, 1.8, and 3.6 μm. Because decays are not exponential, we use the grating decay time τ_G (defined as time when DE decreases to 1/e of its initial intensity) in the analysis. The τ_G increased for the larger grating periods, indicating the contribution of diffusion to the grating decay. The decay curves were measured and τ_G were determined for several excitation intensities, and the inverse decay time $1/\tau_G$ is plotted vs. Λ^{-2} in Fig. 5(c). In this way, the impact of diffusion and recombination was separated, and the plot provided the values of D and carrier lifetime τ_R at high excitation conditions. We note the strong dependence of the bipolar diffusion coefficient on excess carrier density [Fig. 5(b)]. Increase of D vs. excitation was also observed in SiC[50] and GaN,[51] and this effect has been attributed to the many-body interaction in high-density carrier plasma.[50] For CdTe, we fitted D(ΔN) dependence accounting for carrier degeneracy (the first term in brackets) and bandgap renormalisation (the second term in brackets)[50]

$$D(\Delta N) = D_0 \frac{F_{3/2,1}}{F_{3/2}} \left(\frac{F_{1/2}}{F_{-1/2}} - \frac{\Delta N}{kT} \frac{d\Delta E_V}{d\Delta N} \right),$$

$$F_{i,j} = \int_0^\infty x^i \tau_S^j f(x - x_f) dx. \tag{9}$$

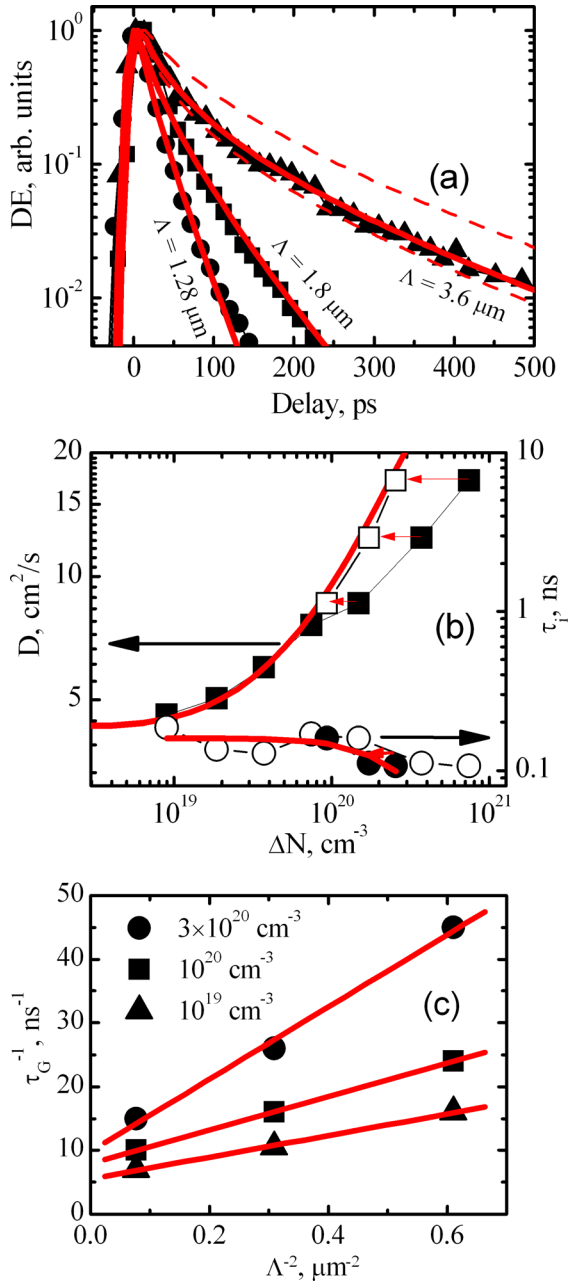

FIG. 5. (a) Diffraction efficiency DE of LITG decay at different grating periods Λ (indicated in the legend) at $\Delta N = 1.5 \times 10^{19}\,\mathrm{cm}^{-3}$. The solid lines are the calculated grating kinetics with $S = 6 \times 10^5$ cm/s. The upper and lower dashed lines are calculated for $S = 2 \times 10^5$ and 2×10^6 cm/s. (b) Excitation-dependent diffusion coefficient D and the recombination time τ_i. The arrows for D indicate corrections for excitation absorption saturation. (c) τ_G^{-1} vs. Λ^{-2} plot for $\Delta N = 10^{19}$, 10^{20} and $3 \times 10^{20}\,\mathrm{cm}^{-3}$.

Here, F_i are the Fermi integrals, $d\Delta E_V/d\Delta N$ is the valence band renormalisation factor, and τ_S is the scattering time by phonons. Here, D_0 is the initial value at low excitations, while its increase with excitation was accounted by the $F_{3/2,1}/F_{3/2}$ factor (it was set to unity in the nondegenerate case by normalizing τ_S), calculated taking into account acoustic and polar optical phonon scattering (dominant with 22 meV phonon energy)[52] and using conductivity masses $m_e = 0.11$ and $m_h = 0.4$.[53] Using $\mu_h = 107\,\mathrm{cm}^2/\mathrm{V\,s}$ and $\mu_e = 1045\,\mathrm{cm}^2/\mathrm{V\,s}$ in low doped and noncompensated CdTe,[54] the maximum value of $D_0 = 5.04\,\mathrm{cm}^2/\mathrm{s}$ was

obtained, being very close to the ambipolar diffusion coefficient D_a, determined by LITG at density $2 \times 10^{18}\,cm^{-3}$ [see Fig. 2(b)].

Fitting of D(ΔN) dependence in Fig. 5(b) revealed that increase is mainly governed by the degeneracy of holes, as $D_{meas} \sim 2D_h$. For the fit we used, $N_{DOS} = 2 \times 10^{19}\,cm^{-3}$, providing $m_{Hdos} = 0.8\ m_0$ [$m_{hh} = 0.7\ m_0$ for CdTe (Ref. 52)] and $D_0 = 4.9\,cm^2/s$. Valence band renormalization impact, in contrary, leads to reduction of the hole diffusion coefficient due to the spatial modulation of the valence band: the relationship $\Delta E_V = 12\,meV \times (N/10^{18})^{1/4}$ points that additional barriers for hole diffusion up to 21–38 meV at $10^{19-20}\,cm^{-3}$ can appear because of bandgap shrinking in the grating maxima. The competition of both mechanisms takes place but the impact of degeneracy was found to be stronger and led to gradual increase of D_a with excitation. However, fit at the highest excitations starts to deviate from the experimental data. It was explained by the absorption saturation, i.e., the generated carrier density does not become proportional to the excitation fluence. Using $1.3 \times 10^{20}\,cm^{-3}$ carrier density, we obtain the electron Fermi level at 0.86 eV above the conduction band minimum, which equals to $h\nu(527\,nm) - E_G$ difference. Thus, absorption should start to saturate, causing a kink in the D(ΔN) dependence at $\sim 10^{20}\,cm^{-3}$ [Fig. 5(b)]. Nevertheless, the carrier density still increases but with the saturating average absorption coefficient $\alpha(\Delta N) = \alpha_0/(1 + \Delta N/N_{sat})^{1/2}$,[55] where we obtain a saturated carrier density of $1.0 \times 10^{20}\,cm^{-3}$.

In turn, we ascribed the further decrease of the surface-recombination governed lifetime $\tau_{0i} = (160 \pm 30)$ ps down to 100 ps [see Fig. 5(b)] to impact of Auger recombination. Fitting of the lifetime excitation dependence with the $1/\tau_i = 1/\tau_{0i} + C\Delta N^2$ relationship, we determined the Auger coefficient $C = (6 \pm 3) \times 10^{-32}\,cm^6/s$. This value is comparable to the estimated one, $C \sim 2 \times 10^{-32}\,cm^6/s$, for bulk CdTe.[56,57]

Modeling of LITG kinetics in Fig. 5(a) with the parameters determined earlier (D, Sec. III A, and τ, Sec. III B) and their dependence on the excitation allowed us to analyze the surface recombination velocity S, which plays an essential role when 1P excitation is near the surface. Numerical solution of the continuity equation [Eq. (10)] was performed applying the boundary condition $D_a\,\delta\Delta N(0,t)/\delta z = S\Delta N(0,t)$ at the front surface (z = 0)[58]

$$\frac{\partial \Delta N(z,t)}{\partial t} = \nabla\left(D(\Delta N)\nabla\Delta N(z,t)\right) - \frac{\Delta N(z,t)}{\tau_R} - B(\Delta N)\Delta N^2(z,t) + G(z,t), \quad (10)$$

where $G(z,t)$ is the carrier generation rate. We calculated spatio-temporal carrier dynamics at the lowest surface excitation, when the initial excess carrier density at the surface was of about $1.5 \times 10^{19}\,cm^{-3}$ [see Fig. 5(a)]. $D = 5\,cm^2/s$ [Fig. 2(b)] was used. The numerical fit provided $S = 6 \times 10^5\,cm/s$, which is close to the previously reported values for bulk CdTe of 3×10^5–6×10^5 (Ref. 59) and $S = 2.8 \times 10^5\,cm/s$ (Ref. 15) but larger that the S value obtained from the simplified approximation of PL decay [relation $1/\tau_{PL} = \alpha S$ leads to $S = 1.3 \times 10^5\,cm/s$ (Ref. 5)] This implies that modeling of LITG decay using the correct value of bipolar diffusion coefficient provides accurate determination of S, as it accounts for fast carrier diffusion away from the surface. Moreover, LITG decay is not sensitive to reabsorption of PL emission, which is always present in monitoring PL decays.

IV. CONCLUSIONS

We applied time-resolved differential absorption (FCA) and light induced transient grating (LITG) techniques with 1P and 2P excitation to analyze excitation-dependent charge carrier lifetimes and diffusion coefficients in semi-insulating CdTe. With 2P excitation, the ambipolar diffusion coefficient increased from 2.8 to 4.9 cm^2/s in the 10^{16}–$10^{18}\,cm^{-3}$ carrier density range, which was attributed to the increased carrier mobility due to the screening of ionized impurities and filling of shallow acceptors ascribed to the Er dopant. We observed carrier lifetimes up to 670 ns and diffusion lengths up to 14 μm, which are the highest-reported values for the single-crystal CdTe. The decrease of carrier lifetime from τ = 670 ns to 75 ns at higher excitation was explained by the increased impact of radiative recombination. The corresponding decrease of the carrier diffusion length was from 14 μm to 6 μm. At very high excitations, in the 10^{19}–$10^{20}\,cm^{-3}$ density range, the D value strongly increased from 5 to 20 cm^2/s due to the carrier degeneracy. At 1P excitation, modeling of the in-depth and in-plane carrier dynamics provided the reliable value of the surface recombination velocity $S = 6 \times 10^5\,cm/s$ for the untreated surface.

We find that crystalline CdTe has sufficient charge carrier lifetimes for the high-efficiency II-VI solar cells,[1] but the surface recombination velocity is approximately two-times higher than previously reported.[5,15,59] The high carrier diffusion length determined here would be sufficient for the high efficiency solar cells where carrier collection is due to diffusion. A combination of 1P/2P excitation spectroscopies, such as used here, provides a useful and reliable analysis of CdTe bulk and interface properties.

ACKNOWLEDGMENTS

At NREL, this work was supported by the U.S. Department of Energy under Contract DE-AC36-08-GO28308 with the National Renewable Energy Laboratory. The U.S. Government retains and the publisher, by accepting the article for publication, acknowledges that the U.S. Government retains a nonexclusive, paid up, irrevocable, worldwide license to publish or reproduce the published form of this work, or allow others to do so, for U.S. Government purposes.

[1] A. Kanevce, M. O. Reese, T. M. Barnes, S. A. Jensen, and W. K. Metzger, J. Appl. Phys. **121**, 214506 (2017).
[2] D. Krasikov and I. Sankin, J. Mater. Chem. A **5**, 3503 (2017).
[3] J. M. Burst, J. N. Duenow, D. S. Albin, E. Colegrove, M. O. Reese, J. A. Aguiar, C.-S. Jiang, M. K. Patel, M. M. Al-Jassim, D. Kuciauskas, S. Swain, T. Ablekim, K. G. Lynn, and W. K. Metzger, Nat. Energy **1**, 16015 (2016).
[4] T. Ablekim, S. K. Swain, W.-J. Yin, K. Zaunbrecher, J. Burst, T. M. Barnes, D. Kuciauskas, S.-H. Wei, and K. G. Lynn, Sci. Rep. **7**, 4563 (2017).

[5]D. Kuciauskas, A. Kanevce, P. Dippo, S. Seyedmohammadi, and R. Malik, "Minority-carrier lifetime and surface recombination velocity in single-crystal CdTe," IEEE J. Photovoltaics **5**, 366–371 (2015).
[6]E. S. Barnard, E. T. Hoke, S. T. Connor, J. R. Groves, T. Kuykendall, Z. Yan, E. C. Samulon, E. D. Bourret-Courchesne, S. Aloni, P. J. Schuck, C. H. Peters, and B. E. Hardin, "Probing carrier lifetimes in photovoltaic materials using subsurface two-photon microscopy," Sci. Rep. **3**, 2098 (2013).
[7]X.-H. Zhao, M. J. DiNezza, S. Liu, C. M. Campbell, Y. Zhao, and Y.-H. Zhang, "TRPL determination of CdTe bulk carrier lifetime and interface recombination velocity of CdTe/MgCdTe double heterostructures grown by molecular beam epitaxy," Appl. Phys. Lett. **105**, 252101 (2014).
[8]P. B. Klein, J. Appl. Phys. **103**, 033702 (2008).
[9]P. Ščajev, V. Gudelis, K. Jarašiūnas, and P. B. Klein, "Fast and slow carrier recombination transients in highly excited 4H- and 3C-SiC crystals at room temperature," J. Appl. Phys. **108**, 023705 (2010).
[10]J.-H. Yang, L. Shi, L.-W. Wang, and S.-H. Wei, "Non-radiative carrier recombination enhanced by two-level process: A first-principles study," Sci. Rep. **6**, 21712 (2016).
[11]K. Jarasiunas, L. Bastiene, J.-C. Launay, P. Delaye, and G. Roosen, "Role of charge state of deep vanadium impurity and associations of defects on optical nonlinearities in semi-insulating CdTe crystals," Semicond. Sci. Technol. **14**, 48–57 (1999).
[12]A. Castaldini, A. Cavallini, B. Fraboni, P. Fernandez, and J. Piqueras, J. Appl. Phys. **83**, 2121 (1998).
[13]J. M. Burst, S. B. Farrell, D. S. Albin, E. Colegrove, M. O. Reese, J. N. Duenow, D. Kuciauskas, and W. K. Metzger, "Carrier density and lifetime for different dopants in single-crystal and polycrystalline CdTe," APL Mater. **4**, 116102 (2016).
[14]T. Ablekim, S. K. Swain, J. McCoy, and K. G. Lynn, "Defects in undoped p-type CdTe single crystals," IEEE J. Photovoltaics **6**, 1663–1667 (2016).
[15]D. Kuciauskas, S. Farrell, P. Dippo, J. Moseley, H. Moutinho, J. V. Li, A. M. A. Motz, A. Kanevce, K. Zaunbrecher, T. A. Gessert, D. H. Levi, W. K. Metzger, E. Colegrove, and S. Sivananthan, "TRPL charge-carrier transport and recombination in heteroepitaxial CdTe," J. Appl. Phys. **116**, 123108 (2014).
[16]A. David and M. J. Grundmann, "Droop in InGaN light-emitting diodes: A differential carrier lifetime analysis," Appl. Phys. Lett. **96**, 103504 (2010).
[17]E. Kioupakis, Q. Yan, D. Steiauf, and C. G. Van de Walle, "Temperature and carrier-density dependence of Auger and radiative recombination in nitride optoelectronic devices," New J. Phys. **15**, 125006 (2013).
[18]H. Zhao and E. A. Schiff, "A light-trapping metric for solar cells with application to cadmium telluride and silicon," IEEE J. Photovoltaics **5**, 487–494 (2015).
[19]T. Malinauskas, K. Jarašiūnas, S. Miasojedovas, S. Juršėnas, B. Beaumont, and P. Gibart, Appl. Phys. Lett. **88**, 202109 (2006).
[20]D. Kuciauskas, A. Kanevce, J. M. Burst, J. N. Duenow, R. Dhere, D. S. Albin, D. H. Levi, and R. K. Ahrenkiel, IEEE J. Photovoltaics **3**, 1319 (2013).
[21]C. A. Hoffman, K. Jarašiūnas, H. J. Gerritsen, and A. Nurmikko, Appl. Phys. Lett. **33**, 536 (1978).
[22]T. Malinauskas, R. Aleksiejūnas, K. Jarašiūnas, B. Beaumont, P. Gibart, A. Kakanakova-Georgieva, E. Janzen, D. Gogova, B. Monemar, and M. Heuken, J. Cryst. Growth **300**, 223 (2007).
[23]P. Ščajev, J. Hassan, K. Jarašiūnas, M. Kato, A. Henry, and J. P. Bergman, "Comparative studies of carrier dynamics in 3C-SiC layers grown on Si and 4H-SiC substrates," J. Electron. Mater. **40**, 394–399 (2011).
[24]P. Ščajev, V. Gudelis, K. Jarašiūnas, I. Kisialiou, E. Ivakin, M. Nesládek, and K. Haenen, "Carrier recombination and diffusivity in microcrystalline CVD-grown and single-crystalline HPHT diamonds," Phys. Status Solidi A **209**, 1744–1749 (2012).
[25]P. Ščajev, S. Miasojedovas, K. Jarašiūnas, K. Hiramatsu, H. Miyake, and B. Gil, "Excitation-dependent carrier dynamics in Al-rich AlGaN layers and multiple quantum wells," Phys. Status Solidi B **252**, 1043–1049 (2015).
[26]K. Jarasiunas, A. Kadys, R. Aleksiejunas, and T. Malinauskas, "Optical nonlinearities and carrier dynamics in semi-insulating crystals," Phys. Status Solidi C **6**, 2846–2848 (2009).
[27]A. Kadys, K. Jarašiūnas, and D. Verstraeten, "Optical discrimination of deep trap contribution to carrier recombination in semi-insulating crystals," J. Appl. Phys. **106**, 013704 (2009).
[28]F. Bassani, S. Tatarenko, K. Saminadayar, J. Bleuse, N. Magnea, and J. L. Pautrat, "Luminescence characterization of CdTe:In grown by molecular beam epitaxy," Appl. Phys. Lett. **58**, 2651 (1991).
[29]U. Reislohner, N. Achtziger, M. Rub, and W. Witthuhn, "Complex formation at indium donors in p-CdTe," J. Cryst. Growth **159**, 372–375 (1996).
[30]R. Soundararajan, K. Lynn, S. Awadallah, C. Szeles, and S.-H. Wei, "Study of defect levels in CdTe using thermoelectric effect spectroscopy," J. Electron. Mater. **35**, 1333–1340 (2006).
[31]Y. P. Gnatenko, M. S. Furyer, A. P. Bukivskii, L. M. Tarakhan, and R. V. Gamernyk, "Photoluminescence and photoelectric properties of CdTe crystals doped with Er atoms," J. Lumin. **160**, 258 (2015).
[32]D. Kučiauskas, private communication (2017).
[33]K. Jarasiunas, R. Aleksiejunas, T. Malinauskas, V. Gudelis, T. Tamulevicius, S. Tamulevicius, A. Guobiene, A. Usikov, V. Dmitriev, and H. J. Gerritsen, "Implementation of diffractive optical element in four-wave mixing scheme for ex situ characterization of hydride vapor phase epitaxy-grown GaN layers," Rev. Sci. Instrum. **78**, 33901 (2007).
[34]P. Ščajev, K. Jarašiūnas, S. Okur, Ü. Özgür, and H. Morkoç, "Carrier dynamics in bulk GaN," J. Appl. Phys. **111**, 023702 (2012).
[35]R. E. Treharne, A. Seymour-Pierce, K. Durose, K. Hutchings, S. Roncallo, and D. Lane, "Optical design and fabrication of fully sputtered CdTe/CdS solar cells," J. Phys.: Conf. Ser. **286**, 012038 (2011).
[36]P. B. Klein, R. Myers-Ward, K.-K. Lew, B. L. VanMil, C. R. Eddy, D. K. Gaskill, A. Shrivastava, and T. S. Sudarshan, "Recombination processes controlling the carrier lifetime in n−4H–SiC epilayers with low $Z_{1/2}$ concentrations," J. Appl. Phys. **108**, 33713 (2010).
[37]B. Jensen, "Free carrier absorption in n-type CdTe," J. Phys. Chem. Solids **34**, 2235–2245 (1973).
[38]A. A. Said, M. Sheik-Bahae, D. J. Hagan, T. H. Wei, J. Wang, J. Young, and E. W. Van Stryland, "Determination of bound-electronic and free-carrier nonlinearities in ZnSe, GaAs, CdTe, and ZnTe," J. Opt. Soc. Am. B **9**, 405–414 (1992).
[39]D. K. Schroder, *Semiconductor Material and Device Characterization* (Wiley-Interscience Publication, NY, 1990), p. 599, ISBN: 0-471-51104-8.
[40]K. K. Chin, "p-Doping limit and donor compensation in CdTe polycrystalline thin film solar cells," Sol. Energy Mater. Sol. Cells **94**, 1627–1629 (2010).
[41]G. Liaugaudas, P. Ščajev, and K. Jarašiūnas, "Evaluation of photoelectrical parameters of highly compensated 3C-SiC epilayers by nonlinear optical techniques," Semicond. Sci. Technol. **29**, 015004 (2014).
[42]C. H. Swartz, M. Edirisooriya, E. G. LeBlanc, O. C. Noriega, P. A. R. D. Jayathilaka, O. S. Ogedengbe, B. L. Hancock, M. Holtz, T. H. Myers, and K. N. Zaunbrecher, "Radiative and interfacial recombination in CdTe heterostructures," Appl. Phys. Lett. **105**, 222107 (2014).
[43]A. Lastras-Martínez, P. M. Raccah, and R. Triboulet, "Minority carrier diffusion length measurements in CdTe by a photocurrent technique," Appl. Phys. Lett. **36**, 469 (1980).
[44]D. R. Wight, D. Bradley, G. Williams, M. Astles, S. J. C. Irvine, and C. A. Jones, "Minority carrier diffusion length in CdTe," J. Cryst. Growth **59**, 323–331 (1982).
[45]L. Tarricone, N. Romeo, G. Sberveglieri, and S. Mora, "Electron and hole diffusion length investigation in CdTe thin films by SPV method," Sol. Energy Mater. **7**, 343–350 (1982).
[46]B. Ridley, *Quantum Processes in Semiconductors* (Clarendon Press, Oxford, 1982).
[47]N. G. Nilsson, "An accurate approximation of the generalized Einstein relation for degenerate semiconductors," Phys. Status Solidi A **19**, K75 (1973).
[48]A. P. Kirk, M. J. DiNezza, S. Liu, X.-H. Zhao, and Y.-H. Zhang, "CdTe vs. GaAs solar cells—A modeling case study with preliminary experimental results," in *Proceedings of the IEEE 39th Photovoltaic Specialists Conference* (2013), pp. 2515–2517.
[49]A. Dmitriev and A. Oruzheinikov, "The rate of radiative recombination in the nitride semiconductors and alloys," J. Appl. Phys. **86**, 3241–3246 (1999).
[50]P. Ščajev and K. Jarašiūnas, "Temperature- and excitation-dependent carrier diffusivity and recombination rate in 4H-SiC," J. Phys. D: Appl. Phys. **46**, 265304 (2013).
[51]T. Malinauskas, K. Jarašiūnas, M. Heuken, F. Scholz, and P. Bruckner, Phys. Status Solidi C **6**, S743 (2009).

[52]D. Kranzer, "Hall and drift mobility of polar p-type semiconductors: II. Application to ZnTe, CdTe, and ZnSe," J. Phys. C: Solid State Phys. **6**, 2977–2987 (1973).
[53]A. Rubio-Ponce, D. Olguin, and I. Hernandez-Calderon, "Calculation of the effective masses of II-VI semiconductor compounds," Superficiesy Vacio **16**, 26–28 (2003), ISSN: 1665-3521.
[54]L. I. Berger, *Semiconductor Materials* (CRC Press, 1996), ISBN: 0849389127, 9780849389122.
[55]R. K. Jain and M. B. Klein, "*Degenerate four-wave mixing in semiconductors,*" in *Optical Phase Conjugation* (Academic Press, Inc., 1983), Chap. 10, ISBN: 0-12-257740-X.
[56]K. A. Bulashevich and S. Y. Karpov, "Is Auger recombination responsible for the efficiency rollover in III-nitride light-emitting diodes?," Phys. Status Solidi C **5**, 2066–2069 (2008).
[57]H. Wen, B. Pinkie, and E. Bellotti, "Direct and phonon-assisted indirect Auger and radiative recombination lifetime in HgCdTe, InAsSb, and InGaAs computed using Green's function formalism," J. Appl. Phys. **118**, 015702 (2015).
[58]M. Boulou and D. Bois, J. Appl. Phys. **48**, 4713 (1977).
[59]K. Suzuki and H. Shiraki, "Evaluation of surface recombination velocity of CdTe radiation detectors by time-of-flight measurements," IEEE Trans. Nucl. Sci. **56**, 1712–1716 (2009).